Journal of Magnetic Resonance 209 (2011) 261–268

Contents lists available at ScienceDirect

Journal of Magnetic Resonance

journal homepage: www.elsevier.com/locate/jmr

Sweep direction and efficiency of the swept-frequency two pulse phase modulated scheme for heteronuclear dipolar-decoupling in solid-state NMR

Subhradip Paul [a], C. Vinod Chandran [b], T. Bräuniger [b], P.K. Madhu [a,*]

[a] Department of Chemical Sciences, Tata Institute of Fundamental Research, Homi Bhabha Road, Colaba, Mumbai 400 005, India
[b] Max-Planck-Institute for Solid State Research, Heisenbergstr. 1, 70569 Stuttgart, Germany

ARTICLE INFO

Article history:
Received 30 November 2010
Revised 14 January 2011
Available online 31 January 2011

Keywords:
Solid-state NMR
Heteronuclear dipolar decoupling
Magic-angle spinning
TPPM
SPINAL
SW_f-TPPM
Floquet theory

ABSTRACT

We present here a bimodal Floquet theoretical and experimental investigation of the direction of sweep in the swept-frequency two pulse phase modulated (SW_f-TPPM) scheme used for heteronuclear dipolar decoupling in solid-state NMR. The efficiency of the decoupling turns out to be independent of the sweep direction.

1. Introduction

The combination of heteronuclear dipolar decoupling sequences and magic angle spinning (MAS) has proven to be essential for acquiring high resolution spectra of rare nuclei like ^{13}C, which are dipolar coupled to abundant spins like ^{1}H or ^{19}F [1]. Initially continuous-wave (CW) irradiation of high RF amplitude (ν_1) was used for decoupling [2] till the introduction of two pulse phase modulation (TPPM) by Bennett et al. which was a significant milestone as it led to considerable increase in efficiency of heteronuclear decoupling [3]. Theoretical and experimental investigation into the modification of the basic unit of TPPM to improve its heteronuclear decoupling efficiency resulted in introduction of frequency and/or phase modulation which led to sequences like FMPM and AMPM [4,5]. Fung and co-workers introduced a sequence called SPINAL which involved incremental phase alteration of four units of TPPM [6]. A supercycled version of this sequence, namely SPINAL-64 found wide range application in the field of heteronuclear decoupling in solid-state NMR [6,7].

Recently, another sequence was introduced which involved an adiabatic sweep over 11 pulse pairs of TPPM by varying the pulse lengths of each pair of TPPM according to a tangential function [8]. This version is called SW_f-TPPM. Variants of SW_f-TPPM and swept SPINAL-64 have been introduced recently [9,10]. Extensive experimental investigations and theoretical calculations have been done to prove that SW_f-TPPM is indeed better than the other decoupling sequences in terms of sensitivity or robustness with respect to the experimental conditions like pulse lengths, offset, and/or MAS frequency [8,11–14].

For SW_f-TPPM the pulse lengths for the 11 pair of pulses are varied by multiplying the pulse length of the TPPM unit by a factor which varies symmetrically around unity. Originally the factors were varied according to a tangential function with the shortest pulse pair being the first unit and the longest being the last unit of the sequence [8]. Later it was found out that linear sweeps perform equally well[9]. In principle we can change the direction of the sweep which means that the sweep can be in an increasing fashion (forward sweep) or decreasing fashion (reverse sweep) as schematically shown in Fig. 1. In this work we present theoretical and experimental study on SW_f-TPPM to investigate whether changing the direction of sweep has any effect on the decoupling efficiency.

2. Theory

The focus of this section will be on the formulation and investigation of the properties of different sweeps in the SW_f-TPPM sequence using bimodal Floquet theory [11,15,16]. TPPM consists of repetitive blocks of the form $\tau_\phi\tau_{-\phi}$ where the pulse length τ corresponds to a flip angle of $\approx 180°$. SW_f-TPPM is derived by adding a sweep on the pulse lengths for 11 pairs of TPPM unit as

* Corresponding author. Fax: +91 22 2280 4610.
E-mail address: madhu@tifr.res.in (P.K. Madhu).

1090-7807/$ - see front matter © 2011 Elsevier Inc. All rights reserved.
doi:10.1016/j.jmr.2011.01.019

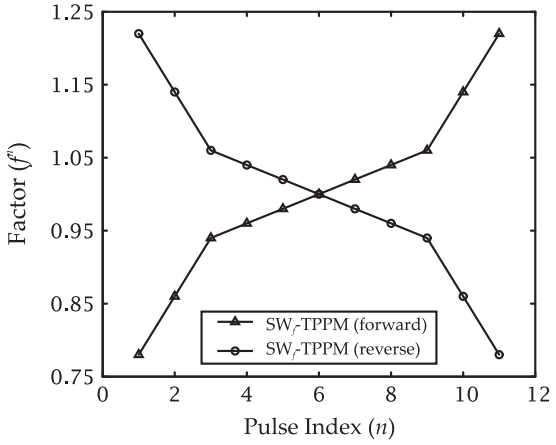

Fig. 1. The multiplication factor (f^n) for the 11 pair of pulses for (a) forward swept SW$_f$-TPPM and (b) reverse swept SW$_f$-TPPM.

mentioned earlier [8]. Here, ϕ corresponds to the phase of the pulses. The SW$_f$-TPPM sequence considered here for the theoretical purpose has the form {[$0.78\tau_\phi$ $0.78\tau_{-\phi}$], [$0.86\tau_\phi$ $0.86\tau_{-\phi}$], [$0.94\tau_\phi$ $0.94\tau_{-\phi}$], [$0.96\tau_\phi$ $0.96\tau_{-\phi}$], [$0.98\tau_\phi$ $0.98\tau_{-\phi}$], [$\tau_\phi\tau_{-\phi}$], [$1.02\tau_\phi$ $1.02\tau_{-\phi}$], [$1.04\tau_\phi$ $1.04\tau_{-\phi}$], [$1.06\tau_\phi$ $1.06\tau_{-\phi}$], [$1.14\tau_\phi$ $1.14\tau_{-\phi}$], [$1.22\tau_\phi$ $1.22\tau_{-\phi}$]} for the forward sweep and {[$1.22\tau_\phi$ $1.22\tau_{-\phi}$], [$1.12\tau_\phi$ $1.14\tau_{-\phi}$], [$1.06\tau_\phi$ $1.06\tau_{-\phi}$], [$1.04\tau_\phi$ $1.04\tau_{-\phi}$], [$1.02\tau_\phi$ $1.02\tau_{-\phi}$], [$\tau_\phi\tau_{-\phi}$], [[$0.98\tau_\phi$ $0.98\tau_{-\phi}$], [$0.96\tau_\phi$ $0.96\tau_{-\phi}$], [$0.94\tau_\phi$ $0.94\tau_{-\phi}$], [$0.86\tau_\phi$ $0.86\tau_{-\phi}$], [$0.78\tau_\phi$ $0.78\tau_{-\phi}$]} for the reverse sweep. Schematic of both the sweep profiles are shown in Fig. 1.

2.1. The interaction frame Hamiltonian

The model that we choose for the purpose of calculation is a spin system in which a single spin (S) of the rare nucleus is dipolar coupled to N abundant spins like protons $I_a(a = 1,2,\ldots,N)$. To express the Hamiltonian of such a system under the influence of both MAS and RF we have to go to the interaction frame of both MAS and RF. The rotating frame representation of such a Hamiltonian under MAS can be represented as [11]:

$$\mathscr{H}(t) = \sum_a \Delta\nu_a I_{0,a}^{(1)} + \sum_{n,a} \sigma_a g_{n,a} I_{0,a}^{(1)} e^{in\nu_r t} + \sum_{n,a} \nu_a G_{n,a} I_{0,a}^{(1)} S_0^{(1)} e^{in\nu_r t} + \nu_1\{\epsilon_{+1} I_1^{(1)} + \epsilon_{-1} I_1^{(1)}\} + \sum_{n,a<b} \nu_{ab} G_{n,ab} I_{0,ab}^{(2)} e^{in\nu_r t} \quad (1)$$

where $I_m^{(l)}$ and $S_m^{(l)}$ are irreducible tensor operators for the angular momentum of the protons and the rare spin respectively. The first term represents the isotropic chemical shift ($\Delta\nu_a$) of the ^{1}H spin whilst the second term represents the anisotropic chemical shift whose strength is given by σ_a and the orientation dependence is given by $g_{n,a}$. The third term represents the heteronuclear dipolar interaction of strength ν_a between the ^{1}H and the S spins. The geometrical dependence of the heteronuclear dipolar coupling is given by $G_{n,a}$. The penultimate term is the time dependent RF field of the decoupling sequence. The final term represents the homonuclear dipolar coupling between the ^{1}H spins, the magnitude of which is given by ν_{ab} whilst the geometrical dependence of the interaction is given by $G_{n,ab}$ [16].

To simplify Eq. (1) we divide the Hamiltonian into two parts according to the eigenstates of the spin operator $S_0^{(1)}$, $\alpha(+)$ and $\beta(-)$ [17]:

$$S_0^{(1)} = \frac{1}{2}\begin{pmatrix} 1 & 0 \\ 0 & -1 \end{pmatrix} = \begin{pmatrix} \alpha(+) & 0 \\ 0 & \beta(-) \end{pmatrix}$$

The resulting Hamiltonian can be written in the spin space of the ^{1}H as:

$$\mathscr{H}^{\pm}(t) = \sum_a \Delta\nu_a I_{0,a}^{(1)} + \sum_{n,a} \sigma_a g_{n,a} I_{0,a}^{(1)} e^{in\nu_r t} + \frac{1}{2}\sum_{n,a} \nu_a G_{n,a} I_{0,a}^{(1)} e^{in\nu_r t} - \frac{1}{2}\sum_{n,a} \nu_a G_{n,a} I_{0,a}^{(1)} e^{in\nu_r t} + \nu_1\{\epsilon_{+1} I_1^{(1)} + \epsilon_{-1} I_1^{(1)}\} + \sum_{n,a<b} \nu_{ab} G_{n,ab} I_{0,ab}^{(2)} e^{in\nu_r t} \quad (2)$$

Eq. (2) can be simplified to

$$\begin{aligned}\mathscr{H}^{\pm}(t) &= \sum_{n,a}(\Delta\nu_a + \sigma_a g_{n,a} e^{in\nu_r t} \pm \frac{1}{2}\nu_a G_{n,a} e^{in\nu_r t}) I_{0,a}^{(1)} + \nu_1\{\epsilon_{+1} I_1^{(1)} + \epsilon_{-1} I_1^{(1)}\} + \sum_{n,a<b} \nu_{ab} G_{n,ab} I_{0,ab}^{(2)} e^{in\nu_r t} \\ &= \sum_{n,a} \Delta\Omega_{n,a}^{\pm} I_{0,a}^{(1)} + \nu_1\{\epsilon_{+1} I_1^{(1)} + \epsilon_{-1} I_{-1}^{(1)}\} + \sum_{n,a<b} \nu_{ab} G_{n,ab} I_{0,ab}^{(2)} e^{in\nu_r t}\end{aligned} \quad (3)$$

where

$$\Delta\Omega_{n,a}^{\pm} = \Delta\nu_a + \sigma_a g_{n,a} e^{in\nu_r t} \pm \frac{1}{2}\nu_a G_{n,a} e^{in\nu_r t}$$

For each of these Hamiltonians a time-dependent evolution operator can be defined in the proton space which is of the form

$$U^{\pm}(t) = T\exp\{-i\int_0^t \mathscr{H}^{\pm}(\tau)d\tau\} \quad (4)$$

The ideal decoupling condition is achieved when the S spin signal is not modulated by the evolution operator from the I spins, a condition which can be achieved when $U^{+}(t) \approx U^{-}(t)$.

The pulse sequences are all cyclic and comprise of elements of overall duration τ_c, which repeats itself in the time-domain. This introduces the second time dependence in the Hamiltonian ($\mathscr{H}^{\pm}$) given by Eq. (3), which shows another periodicity with a characteristic frequency ν_c. So the Hamiltonian is modulated by two frequencies ν_r and ν_c which are not necessarily commensurate. Average Hamiltonian Theory [18] cannot deal with two such incommensurate time dependencies simultaneously. So to understand the properties of decoupling here we have to rely on bimodal Floquet theory which allows us to derive an effective Hamiltonian for a spin system experiencing two time dependencies simultaneously [16]. In order to refrain from going into a third time-dependency [19], the sequences described here are all of constant amplitude but phase modulated. In the rotating frame we have an irradiation which has oscillating components along ±xz-plane as shown in Fig. 2a. We choose an interaction frame which corresponds to a CW irradiation of constant amplitude in the y direction in the rotating frame as shown in Fig. 2a. This irradiation has an amplitude $\nu_{int} = q\nu_c$ whose magnitude should be as close as possible to the actual RF amplitude with the criterion, $|\nu_1 - q\nu_c| < 0.5\nu_c$. A transformation to the RF interaction frame leaves a small component along the y direction and components in the ±xz plane as shown in Fig. 2b. The Hamiltonian in the interaction frame can be expressed as:

$$\widetilde{\mathscr{H}}^{\pm}(t) = \sum_{m,n,k,a} \Delta\Omega_{n,a}^{\pm} d_{m,k}^{(1)} I_{m,a}^{(1)} e^{in\nu_r t} e^{ik\nu_c t} + \sum_{m,n,k,a<b} \nu_{ab} G_{n,ab} d_{m,k}^{(2)} I_{m,ab}^{(2)} e^{in\nu_r t} e^{ik\nu_c t} + \sum_{m,k} \nu_1 \epsilon_{m,k} I_m^{(1)} e^{ik\nu_c t} \quad (5)$$

The Fourier coefficients $d_{m,k}^{(1)}$ and $d_{m,k}^{(2)}$ are defined by the frame transformation followed by a Fourier expansion

$$e^{-i\nu_{int} I_y t} I_0^{(l)} e^{i\nu_{int} I_y t} = d_{m,k}^{(l)} I_m^{(l)} e^{ik\nu_c t} \quad (6)$$

where $k/q = 0, \pm1$ for $l = 1$ and $k/q = 0, \pm1, \pm2$ for $l = 2$. The Fourier coefficients $\epsilon_{m,k}$ are defined by the Fourier expansion which follows the frame transformation

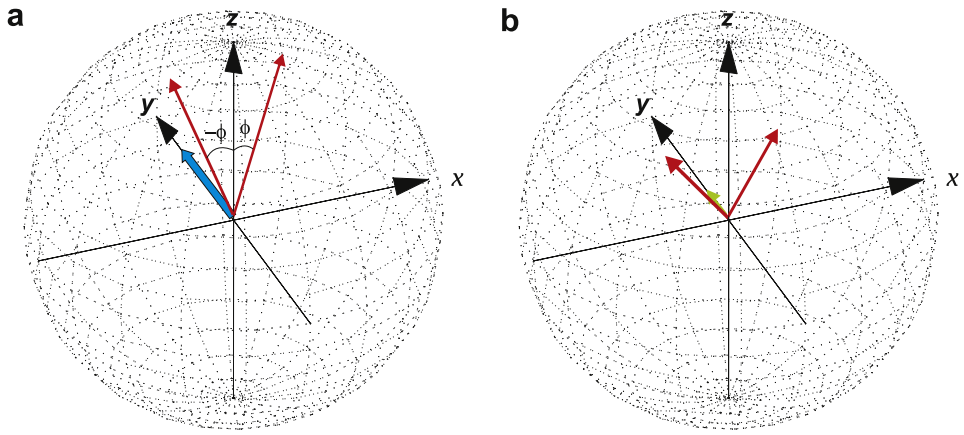

Fig. 2. Schematic representation of the CW interaction frame of constant amplitude in *y*-direction and the RF components in both the (a) rotating and the (b) interaction frame. (a) In the rotating frame the RF components oscillates in the *xz* plane with an angle ϕ and RF amplitude ν_1 (shown by red arrow). The interaction frame is represented by an RF irradiation of constant amplitude ($\nu_{int} = q\nu_c$) pointing in the *y*-direction (shown by blue arrow). (b) Transformation to the interaction frame results in a residual field in the *xz*-plane (shown by red arrow) whilst a small residual component is left behind in the *y*-direction (shown by green arrow). (For interpretation of the references to colour in this figure legend, the reader is referred to the web version of this article.)

$$\begin{aligned}
&\nu_1 e^{-i\nu_{int}I_y t}\{\epsilon_{+1}(t)I_{+1} + \epsilon_{-1}(t)I_{-1} + \nu_{int}I_y\}e^{i\nu_{int}I_y t}\\
&= \nu_1 e^{-i\nu_{int}I_y t}\left\{\epsilon_{+1}(t)I_{+1} + \epsilon_{-1}(t)I_{-1} + \frac{i}{2}\nu_{int}(I_{+1} - I_{-1})\right\}e^{i\nu_{int}I_y t}\\
&= \sum_{m,k}\epsilon_{m,k}I_m^{(1)}e^{ik\nu_c t} \qquad (7)
\end{aligned}$$

Here, k runs from $-\infty$ to $+\infty$.

2.2. Floquet Hamiltonian and van Vleck transformation

In order to derive the decoupling conditions we have to make the Hamiltonian time independent and then diagonalise it. The first step involves expressing the Hamiltonian in the Floquet space which removes the time-dependency from the Hamiltonian but makes it infinite dimensional whilst the second step involves either direct diagonalisation or some transformation which can generate approximate block diagonals. The interaction frame Hamiltonian from Eq. (5) can be written in the Floquet representation as

$$\mathscr{H}_F^{\pm} = \sum_{n,k}\mathscr{H}_{nk}^{\pm}F_n^r F_k^c + \nu_r N^r + \nu_c N^c \qquad (8)$$

where

$$\mathscr{H}_{nk}^{\pm} = \sum_{m,n,k,a}\Delta\Omega_{n,a}^{\pm}d_{m,k}^{(1)}I_{m,a}^{(1)} + \sum_{m,n,k,a<b}\nu_{ab}G_{n,ab}d_{m,k}^{(2)}I_{m,ab}^{(2)} + \sum_{m,k}\nu_1\epsilon_{m,k}I_m^{(1)} \qquad (9)$$

and, F and N are the number and the ladder operators respectively [20]. The number and ladder operators, and $\mathscr{H}_{nk}^{\pm}$ are shown in the matrix form in Figs. 3 and 4 respectively.

Inspection of the Hamiltonian given by Eq. (9) reveals that the first term containing $\Delta\Omega_{n,a}^{\pm}$ creates the difference between $\mathscr{H}_F^{+}$ and $\mathscr{H}_F^{-}$. The RF modulation comes from the second term. The purpose is to generate $\epsilon_{m,k}$ coefficients which can minimise the difference between the Hamiltonians so that the condition $U^{+}(t) \approx U^{-}(t)$ is achieved. A van Vleck transformation [21] is then applied which generates block-diagonals in the Fourier space where the off-diagonal blocks are small and can be ignored. We also ignore here the off-diagonal blocks generated by the homonuclear couplings by putting $\nu_{ab} = 0$. These can be treated separately as shown in Ref. [11].

The van Vleck transformation can be done in two steps. Firstly the transformation is done on the first term in Eq. (9) containing the heteronuclear dipolar terms. For sequences with very small $\nu_1\epsilon_{mk}, k \neq 0$, their off-diagonal elements $(\nu_1\epsilon_{mk}F_0^r F_k^c)$ can be ignored, but with increasing magnitude of these elements, an additional van Vleck transformation is performed. For some decoupling sequences, like SW$_f$-TPPM at high ν_1 and ϕ, it may so happen that the magnitude of the elements $\nu_1\epsilon_{mk}$ becomes of the order of or higher than ν_c. In such a situation, the van Vleck transformation cannot be performed and direct diagonalisation is the only way. We have not gone into the regime of high RF amplitude and phase values in the present work and hence van Vleck transformation is sufficient to generate the approximate block diagonals.

The first van Vleck transformation is done on elements arising from the first term in Eq. (9). Leaving the off-diagonal RF elements untouched, the block diagonalised Floquet Hamiltonian containing only zero- and first-order terms can be written as:

$$\begin{aligned}
\Lambda_F^{\pm} \approx \{&\widetilde{\mathscr{H}}_{00}^{rf} + \widetilde{\mathscr{H}}_{00}^{(\delta-IS)-rf(\pm)} + \widetilde{\mathscr{H}}_{00}^{(\delta-IS)(\pm)}\}F_0^r F_0^c + \mathscr{H}_{0k}^{rf}F_0^r F_k^c\\
&+ \nu_r N^r + \nu_c N^c \qquad (10)
\end{aligned}$$

where

$$\begin{aligned}
\widetilde{\mathscr{H}}_{00}^{rf} &= \sum_m \nu_1\epsilon_{m,0}I_m^{(1)}\\
\widetilde{\mathscr{H}}_{00}^{(CS-IS)-rf(\pm)} &= -\frac{1}{2}\sum_{a,m,m',k\neq 0}\Delta\Omega_{0,a}^{\pm}\nu_1\frac{d_{m,k}^{(1)}\epsilon_{m',-k}}{k\nu_c}[I_m^{(1)}, I_{m'}^{(1)}] \qquad (11)\\
\widetilde{\mathscr{H}}_{00}^{(CS-IS)(\pm)} &= -\frac{1}{2}\sum_{a,m,m',n,k\neq 0}\Delta\Omega_{n,a}^{\pm}\Delta\Omega_{-n,a}^{\pm}\frac{d_{m,k}^{(1)}d_{m',-k}^{(1)}}{n\nu_r + k\nu_c}\left[I_m^{(1)}, I_{m'}^{(1)}\right]
\end{aligned}$$

The first term represents contribution from the RF and the second term correlates the CSA term with itself, the heteronuclear dipolar coupling with itself, the cross-term between the two, and the cross-term between the RF, CSA, and heteronuclear dipolar couplings. The third term correlates CSA with itself, heteronuclear dipolar coupling with itself, and the cross-terms between the two. The off-diagonal elements due to the RF are given by

$$\mathscr{H}_{0k}^{rf} = \sum_{m,k}\nu_1\epsilon_{m,k}I_m^{(1)} \qquad (12)$$

A matrix representation of the first and the second term of Eq. (10) is schematically shown in Fig. 5b which is obtained by applying van Vleck transformation on the matrix (Fig. 5a) given by Eq. (9).

The second van Vleck transformation essentially brings the off-diagonal elements as shown in Fig. 5b to the diagonal as schemat-

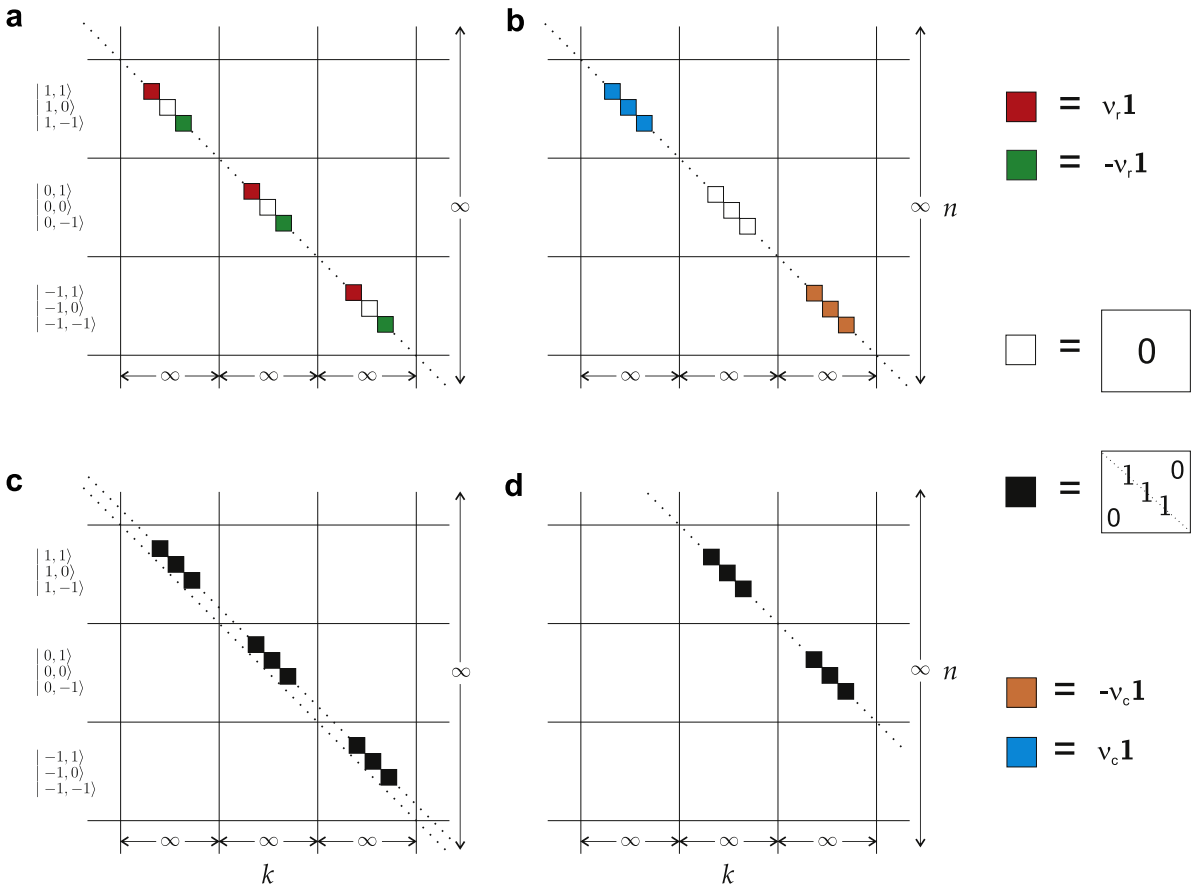

Fig. 3. The matrix representation of the number operators (a) N^c and (b) N^r, and the ladder operators (c) F^c_{-1} and (d) F^r_{-1} in the Fourier states $|n,k\rangle$ with n representing the Fourier states corresponding to the spinning frequency ν_r, and k representing the Fourier states corresponding to the cycle frequency of the RF ν_c. All the matrices shown here are infinite dimensional.

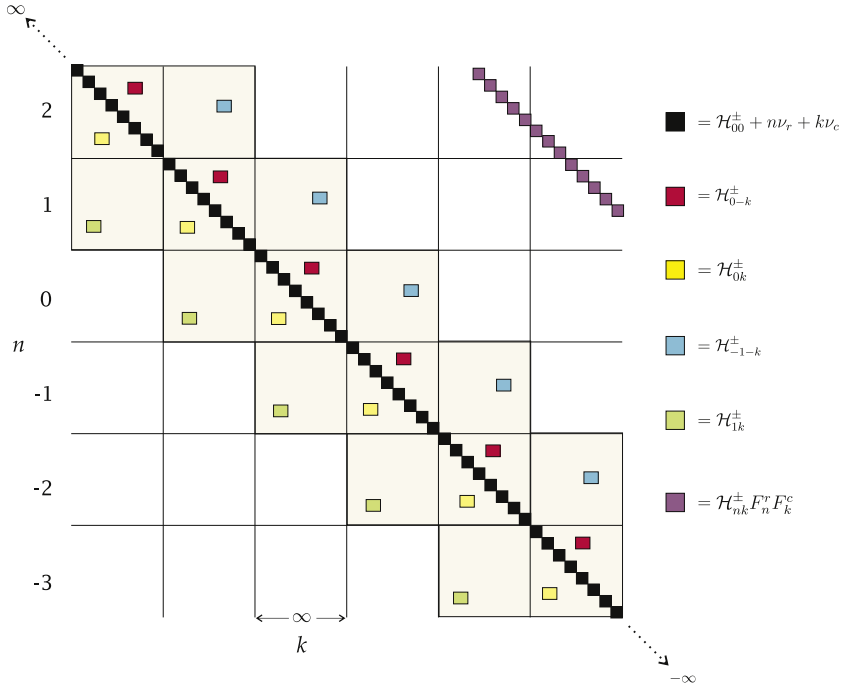

Fig. 4. Different elements of the Floquet Hamiltonian for a spin system experiencing two characteristic frequencies ν_c and ν_r in the matrix representation. The matrix is composed of infinite dimensional blocks ($-\infty \leqslant k \leqslant \infty$) which constitute an infinite-dimensional matrix ($-\infty \leqslant n \leqslant \infty$). The different elements in Eq. (8) are shown in the matrix as indicated on the figure.

ically shown in Fig. 5c. The second van Vleck transformation on $\mathscr{H}_{0k}^{rf}$ results in the Hamiltonian that can be represented as

$$\Lambda_F^{\pm} \approx \{\widetilde{\mathscr{H}}_{00}^{rf} + \widetilde{\mathscr{H}}_{00}^{(\delta-IS)-rf(\pm)} + \widetilde{\mathscr{H}}_{00}^{(\delta-IS)(\pm)}\}F_0^r F_0^c + \nu_r N^r + \nu_c N^c \tag{13}$$

The zero- and first-order terms of $\widetilde{\mathscr{H}}_{00}^{rf}$ in $\mathscr{H}_{eff}^{\pm}$ are given by

$$\widetilde{\mathscr{H}}_{eff}^{rf} = \sum_m \nu_1 \epsilon_{m,0} I_m^{(1)} - \frac{\nu_1^2}{2} \sum_{m,m',k\neq 0} \frac{\epsilon_{m,k}\epsilon_{m',-k}}{k\nu_c}[I_m^{(1)}, I_{m'}^{(1)}] \tag{14}$$

To understand the decoupling condition and to simplify the expressions we convert the irreducible tensor representations to linear angular momentum operators using the following relations:

$$\begin{aligned}
&I_0^{(1)} = I_z && d_{0,k}^{(1)} = d_{z,k} && \epsilon_{0,k} = \epsilon_{z,k} \\
&I_1^{(1)} = -\tfrac{1}{\sqrt{2}}(I_x + iI_y) && d_{1,k}^{(1)} = -\tfrac{1}{\sqrt{2}}(d_{x,k} + id_{y,k}) && \epsilon_{1,k} = -\tfrac{1}{\sqrt{2}}(\epsilon_{x,k} + i\epsilon_{y,k}) \\
&I_{-1}^{(1)} = \tfrac{1}{\sqrt{2}}(I_x - iI_y) && d_{-1,k}^{(1)} = \tfrac{1}{\sqrt{2}}(d_{x,k} - id_{y,k}) && \epsilon_{-1,k} = \tfrac{1}{\sqrt{2}}(\epsilon_{x,k} - i\epsilon_{y,k})
\end{aligned}$$

The effective Hamiltonian in the basis of the linear angular momentum operators for the three terms in Eq. (13) is given by [11]:

$$\begin{aligned}
\widetilde{\mathscr{H}}_{eff}^{rf} &= \sum_p \nu_1 \epsilon_{p,0} I_p - \frac{\nu_1^2}{2} \sum_{p,p',k\neq 0} \frac{\epsilon_{p,k}\epsilon_{p',-k}}{k\nu_c}[I_p, I_{p'}] \\
\widetilde{\mathscr{H}}_{eff}^{(CS-IS)-rf} &= -\frac{1}{2}\sum_a \frac{\Delta\nu_a^2}{q\nu_c} I_y - \sum_{a,p,p',k=\pm q} \Delta\nu_a \nu_1 \frac{d_{p,k}\epsilon_{p',-k}}{k\nu_c}[I_p, I_{p'}] \\
\widetilde{\mathscr{H}}_{eff}^{(CS-IS)\pm} &= -\frac{1}{2}\sum_{a,n\neq 0} \Delta\Omega_{n,a}^{\pm}\Delta\Omega_{-n,a}^{\pm} \frac{q\nu_c}{n^2\nu_r^2 - q^2\nu_c^2} I_y
\end{aligned} \tag{15}$$

The last term in Eq. (15) is the only term which creates the difference between the Hamiltonians $\widetilde{\mathscr{H}}^{+}$ and $\widetilde{\mathscr{H}}^{-}$. This term must be suppressed to minimise the heteronuclear dipolar broadening of the spectra. The term has the linear angular momentum operator I_y. However, a careful look at the other two terms reveals that all the three terms contribute to the magnitude of the coefficient of the linear operators pointing in the y-direction. The contributions coming from these three terms are however, indistinguishable in the Hamiltonian. So the RF should have a minimal y-component and the xz component of the RF must suppress the influence of all the I_y terms.

2.3. The decoupling condition

The decoupling condition is derived from $\widetilde{\mathscr{H}}_{eff}^{rf}$ in Eq. (15). In order to evaluate and verify the decoupling conditions we have carried out simulations on a $^{13}CHH_2$ fragment where, one ^1H is directly bonded to the ^{13}C whilst the other two non-bonded ^1H are dipolar coupled to the carbon through space. We measure the linewidth of the carbon peak as a function of ν_1 and ϕ for the sequence SW$_f$-TPPM. We have done simulations and calculations for the forward and reverse sweeps on pulse lengths of the SW$_f$-TPPM in order to investigate whether change in the direction of the sweep makes any change in the decoupling condition.

Numerical simulations were carried out using the SPINEVOLUTION programme [22]. The RF amplitude is varied in the range of 80–119 kHz and the phase is varied in the range of 5–35°. The linewidth of the ^{13}C peak is plotted as a function of ν_1 and ϕ in Fig. 6. The contour profiles for both the sequences hint that changing the direction of the sweep has no effect on the decoupling efficiency

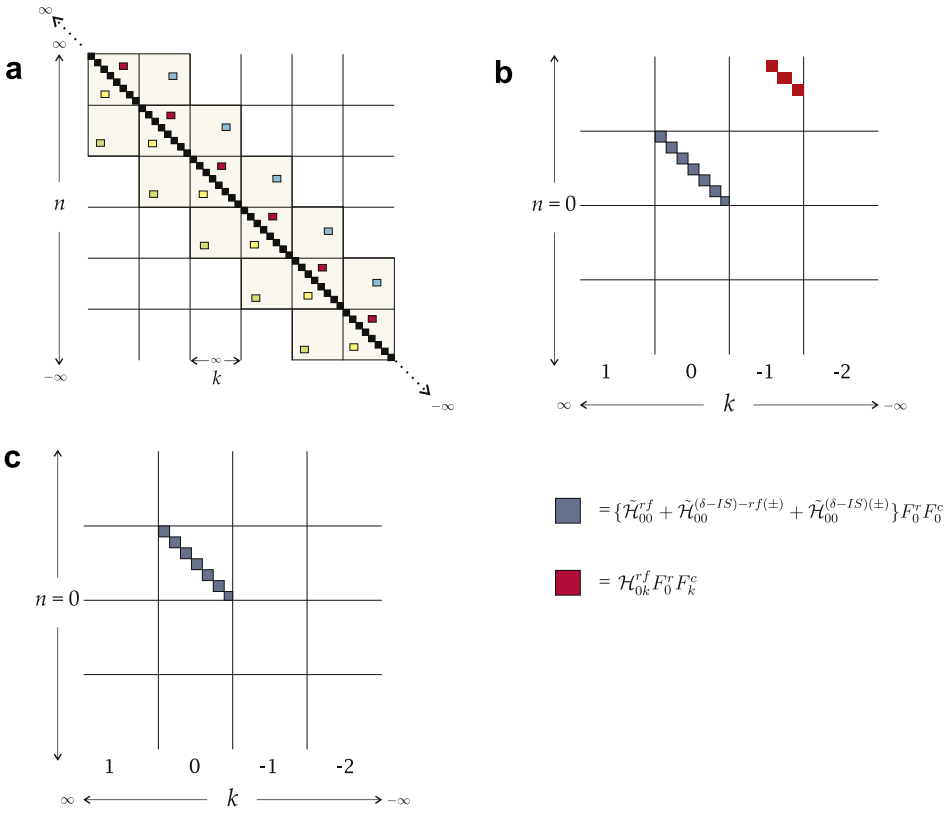

Fig. 5. A schematic representation of the two van Vleck transformations done on (a) $\mathscr{H}_F^{\pm}$ given in Eq. (8). The matrix obtained after the first van Vleck transformation where the transformation is done on the first term in Eq. (9) leaving the $\nu_1\epsilon_{mk}F_0^rF_k^c$ is shown in (b). Both the diagonal elements (grey squares) (first term in Eq. (10)) and off-diagonal elements (red squares) (second term in Eq. (10)) are shown here. (c) Schematic representation of the matrix for the first term in Eq. (13) obtained after the second van Vleck transformation. The final van Vleck results in diagonal elements with k and $n = 0$. (For interpretation of the references to colour in this figure legend, the reader is referred to the web version of this article.)

and this will be corroborated by experimental and theoretical findings.

As mentioned earlier, the part of the effective Hamiltonian $\widetilde{\mathscr{H}}^{rf}_{eff}$ that leads to line broadening is proportional to I_y and these can be eliminated or reduced by *xz*-component coming from $\widetilde{\mathscr{H}}^{rf}_{eff}$. For all the decoupling sequences an RF amplitude can be found out which leads to complete elimination of the *y*-component. So the first criterion for decoupling is the elimination of the *y*-component by choosing proper experimental parameters whilst the quality of the decoupling is then determined by the suppression of the *y*-components by the *xz* -components. The elimination of the *y*-components alone does not serve the purpose of decoupling due to the off-resonance and RF inhomogeneity effects. As a result the suppression of these terms by the *xz*-components is important.

On the contours shown in Fig. 6a and b, the $\nu_1$for the decoupling conditions are plotted at the respective ϕ values where the *y*-component goes to zero for both reverse and forward sweeps of SW$_f$-TPPM. These calculations were done with an interaction frame frequency of ν_{int} = 100 kHz and q = 11. Both the zero- and first-order terms have been included in the calculation and the Fourier coefficients $\epsilon_{p,k}$ have been extracted upto k = 100. From the figure it can be ascertained that the decoupling condition falls on the region where the line width is minimal. For both the forward and reverse sweeps the decoupling condition falls exactly at the same position of the RF amplitude inferring that changing the direction of the sweep does not affect decoupling.

Fig. 7 shows the magnitude of the *xz*-component for both the (a) forward and (b) reverse sweeps of SW$_f$-TPPM at the decoupling condition. The magnitude of the components remains the same irrespective of the direction of the sweep.

Fig. 8 shows the ratio between the magnitude of the *y*-component to that of the component in the *xz*-plane as a function of the RF amplitude for a phase value which is chosen to be ϕ = 15° for both (a) forward and (b) reverse sweeps. For both forward and reverse sweeps the best decoupling is obtained at a pulse length which is slightly higher than that corresponding to a flip angle of 180°.

The direction of the sweep for a decoupling sequence is important because for more complex sequences like SPINAL-64 and recently introduced supercycled version of SW$_f$-TPPM [23], changing the direction of the sweep produces different results. In the SW$_f$-TPPM sequence, only the pulse durations are incrementally changed, whereas the phase angles remain constant. For most implementations of SW$_f$-TPPM, the building block consists of an odd number of pulse pairs (usually 11). Therefore, reversal of the frequency sweep is easily accomplished by an exact inversion of the sequence around the centre pulse pair. Matters are more complex for decoupling sequences where both pulse duration and phase angle are altered within the building block like SW-SPINAL [10]. The addition of small phase angle increments in SPINAL is not done in a fully cyclic manner. This means that the basic building block (often designated by Q) starts and ends with different phase angles, making a symmetric inversion within Q impossible. Furthermore, the Q blocks are assembled into super-cycles of the type $Q\overline{Q}\overline{Q}Q\overline{Q}Q\overline{Q}\overline{Q}$, so sweeps may be defined in different extensions over the Q blocks. Consequently, the behaviour of the SW-SPINAL sequence upon change of sweep direction is more complex. Experimentally and numerically, we found that by inverting the pulse duration increment only (i.e., keeping the phase change pattern as in the forward sweep), the performance tends to deteriorate. However, numerical simulations indicate that also for the "fully" inverted sequence, performance differences between forward and reverse sweeps may occur. A similar complex behaviour is expected for the super-cycled version of SW$_f$-TPPM, which was recently suggested for efficient spin decoupling in liquid crystalline systems [23].

3. Experimental

The experiments were carried out on Bruker 400 MHz spectrometers using a 4 mm triple-resonance probe on commercially available unlabelled L-Tyrosine for proton decoupling and potassium nonafluoro-1-butanesulfonate (NBFS-K) for fluorine decoupling. The molecular structure and assignment of the ^{13}C spectra of NBFS-K are given in Ref. [24].

4. Results and discussions

In order to describe the nature of the sweep used in the experiments we define some parameters as defined earlier in the Ref. [9]. The SW$_f$-TPPM sequences described here consists of q pulse pairs of TPPM where q = 11 for the present work. The pulse duration of the nth pulse ($n = 0,1,2,\ldots,q-1$) is given by $\tau_p^n = f^n\tau_p$. The f^n function defines the nature of the sweep. The functions are defined in Table 1 for the two different directions of sweep and the

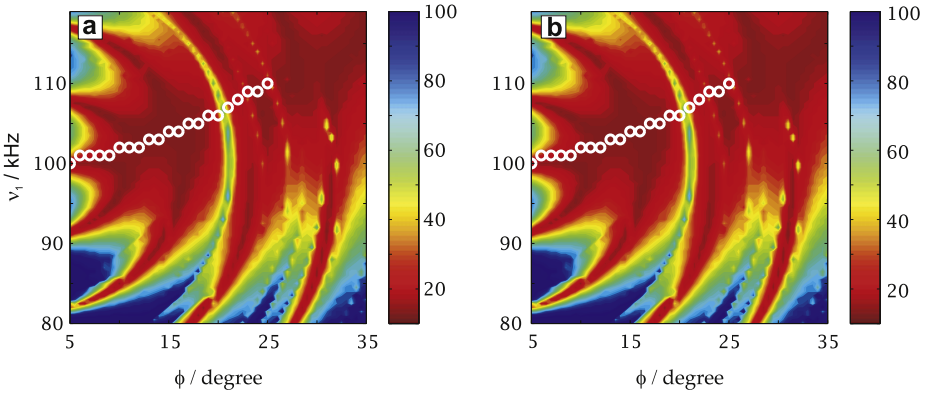

Fig. 6. Simulated line-width of a $^{13}CHH_2$ system obtained with SPINEVOLUTION programme as a function of ν_1 and ϕ for (a) SW$_f$-TPPM with forward sweep and (b) SW$_f$-TPPM with reverse sweep. The isotropic chemical-shift separation between the H and the H_2 system was 2 ppm and the irradiation frequency on the protons was kept on resonance. The fragment has a dipolar coupling strength of 22 kHz between ^{13}C and two of the protons and 10 kHz with the other proton. The simulations were done with 1 kHz CSA on the protons and the ZCW scheme of powder averaging [25–27] with 610 pair of crystallite orientations. The homonuclear couplings have been switched off (see text). The cycle times are 110 μs for both (a) and (b). The spinning frequency was kept at 10 kHz. The phase resolution was 0.5° and the RF amplitude resolution was 0.5 kHz. The dotted line on the contour represents the calculation where the residual field component along I_y has been nullified (see text).

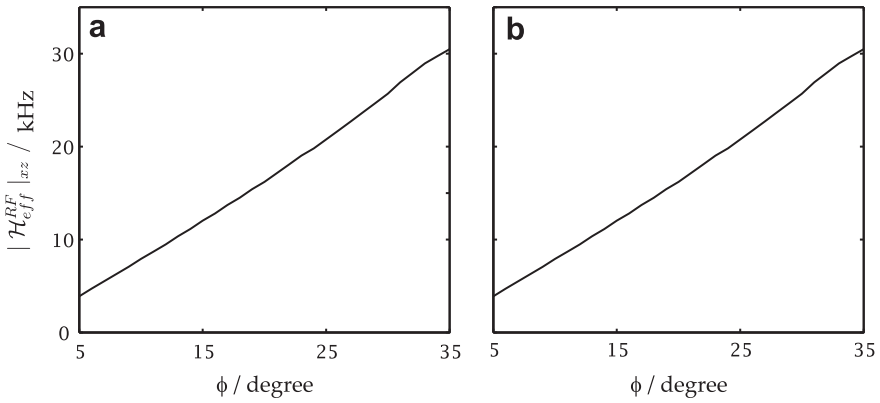

Fig. 7. The magnitude of the component in the *xz*-plane as a function of phases (ϕ) of the pulses for (a) forward swept SW$_f$-TPPM and (b) reverse swept SW$_f$-TPPM at ν_1 where the *y*-component has been nullified as shown in Fig. 5.

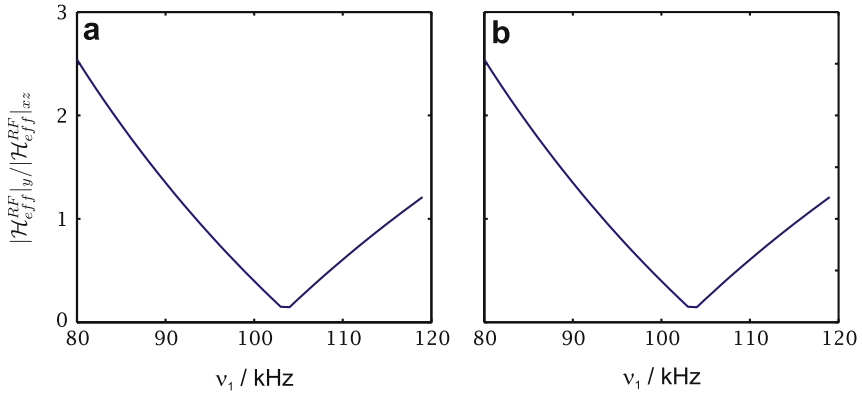

Fig. 8. The ratio of the effective RF field component along *y* to its *xz*-component at ϕ = 15° at different RF amplitudes for (a) forward swept SW$_f$-TPPM and (b) reverse swept SW$_f$-TPPM.

Table 1
Calculation of multiplication factors for the pulses of SW$_f$-TPPM used in the experiment. The cycle constitutes of *q* pair of pulses of alternating phase ϕ and $-\phi$, with f^0 being the factor of the first and f^{q-1} being the factor of the last pair of pulses. The tangent cut-off angle (t_{co}) has to be defined. The actual pulse duration $\tau_p^n$is defined by $\tau_p^n = f^n\tau_p$, where τ_p is the length of one of the pulses in the TPPM unit which has been used to build the SW$_f$-TPPM sequence.

	Functions	Magnitudes
Specified parameters	f^0, f^{q-1}, t_{co}, q	0.60, 1.46, 60°, 11
Functions	$d = f^{q-1} - f^0$	0.80
Defining the sweep	$x = t_{co}(-1 + \frac{2}{q-1}n)$	−48°−36°−24°−12°0° 12°24°36°48°60°72°
Factor for *n*th pulse	$f^n = f^0 + \frac{d}{2}(1 + \frac{\tan x}{\tan t_{co}})$	0.69 0.75 0.79 0.83 0.86
$n = 1,2,\ldots,q-1$		0.89 0.93 0.97 1.04 1.13 1.34

parameters defining the sweep at the experimental condition are enlisted in Table 1.

Fig. 9 shows the intensity of $^{13}CH_2$ peak of tyrosine as a function of the offset on the ^{1}H channel. The spinning frequency is kept at 10 kHz and the RF amplitude used for decoupling is 80 kHz. From the figure it is evident that changing the direction of the sweep has no effect on the efficiency of decoupling.

Fig. 10a and b show the ^{19} F-decoupled ^{13}C spectra of NBFS-K at ν_r = 10 kHz and ν_1 = 80 kHz. The intensity obtained is the same irrespective of the direction of the sweep on the 11 pairs of pulses of SW$_f$-TPPM.

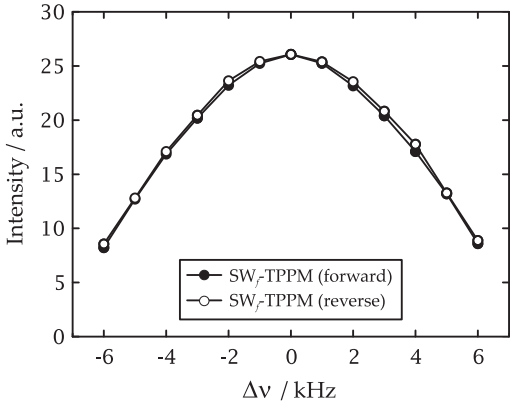

Fig. 9. Offset dependence of the ^{13}C resonance of the CH_2 peak of tyrosine for forward (filled circles) and reverse sweeps (hollow circles) on SW$_f$-TPPM. The offset on the protons was varied in the range of ±6 kHz. The MAS frequency was kept at 10 kHz and the decoupling RF amplitude employed was 80 kHz.

Fig. 11a and b show offset-dependence of the β- and γ-^{13}C peaks of NBFS-K. The offset has been varied on the ^{19}F channel whilst the intensity of the ^{13}C peaks are monitored. The intensity obtained is independent of the direction of the sweep as both forward and reverse SW$_f$-TPPM deliver the same performance.

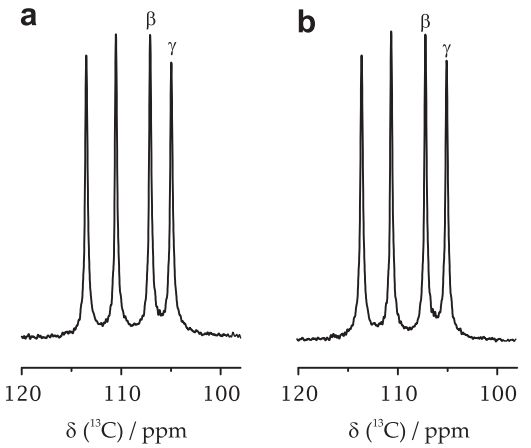

Fig. 10. Spectral comparison of the ^{13}C resonances of the compound NBFS-K obtained by decoupling the ^{19}F abundant spins at ν_r = 10 kHz and ν_1 = 80 kHz. The molecular structure and resonance assignment are given in Ref. [24].

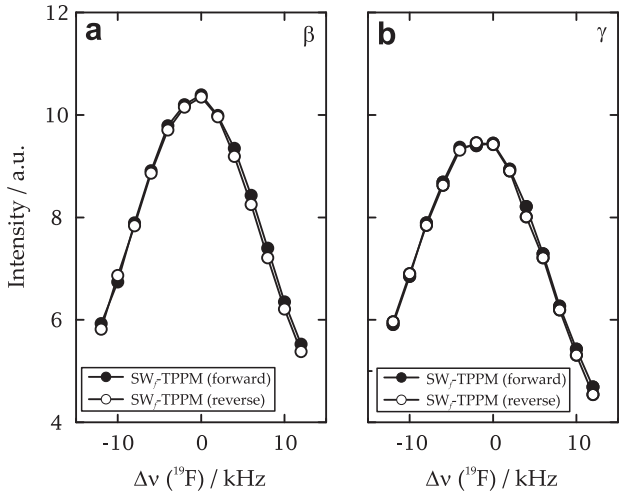

Fig. 11. Offset dependence of the (a) β and (b) γ- ^{13}C resonances NBFS-K for forward (filled circles) and reverse sweeps (hollow circles) on SW$_f$-TPPM. The offset on the protons was varied in the range of ±10 kHz. The MAS frequency was kept at 10 kHz and the decoupling RF amplitude employed was 80 kHz.

5. Conclusions

We have investigated the direction of the sweep in SW$_f$-TPPM sequence using bimodal Floquet theory. We observe that experimental results with modulations, in either pulse duration as in SW$_f$-TPPM or both phase and pulse duration as in Ref. [13] (not shown here), that possess an inversion point of symmetry the direction of sweep does not affect the experimental results. This is established here by theoretical arguments, simulations, and experimental results. Experimental data are presented which involve heteronuclear decoupling of abundant spins like ^{1}H and ^{19}F.

Acknowledgments

We acknowledge the National Facility for High Field NMR, TIFR, Mumbai and financial support by the German Science Foundation (DFG grant BR 3370/4-1). P.K. Madhu acknowledges assistance from Department of Science and Technology, India, for funding under SERC scheme, SR/S1/PC/27/2009.

References

[1] M. Ernst, Heteronuclear spin decoupling in solid-state NMR under magic-angle sample spinning, J. Magn. Reson. 162 (2003) 1.
[2] A.L. Bloom, J.N. Shoolery, Effects of perturbing radiofrequency fields on nuclear spin coupling, Phys. Rev. 97 (1955) 1261.
[3] A.E. Bennett, C.M. Rienstra, M. Auger, K.V. Lakshmi, R.G. Griffin, Heteronuclear decoupling in rotating solids, J. Chem. Phys. 103 (1995) 6951.
[4] K. Takegoshi, J. Mizokami, T. Terao, ^{1}H decoupling with third averaging in solid NMR, Chem. Phys. Lett. 341 (2001) 540.
[5] Z.H. Gan, R.R. Ernst, Frequency- and phase-modulated heteronuclear decoupling in rotating solids, Solid State Nucl. Magn. Reson. 8 (1997) 153.
[6] B.M. Fung, A.K. Khitrin, K. Ermolaev, An improved broadband decoupling sequence for liquid crystals and solids, J. Magn. Reson. 142 (2000) 97.
[7] G.D. Paëpe, D. Sakellariou, P. Hodgkinson, S. Hediger, L. Emsley, Heteronuclear decoupling in NMR of liquid crystals using continuous phase modulation, Chem. Phys. Lett. 368 (2003) 511.
[8] R.S. Thakur, N.D. Kurur, P.K. Madhu, Swept-frequency two-pulse phase modulation for heteronuclear dipolar decoupling in solid-state NMR, Chem. Phys. Lett. 426 (2006) 459.
[9] C.V. Chandran, P.K. Madhu, N.D. Kurur, T. Bräuniger, Swept-frequency two-pulse phase modulation (SW$_f$-TPPM) sequences with linear sweep profile for heteronuclear decoupling in solid-state NMR, Magn. Reson. Chem. 46 (2008) 943.
[10] C.V. Chandran, T. Bräuniger, Efficient heteronuclear dipolar decoupling in solid-state NMR using frequency-swept SPINAL sequences, J. Magn. Reson. 200 (2009) 226.
[11] M. Leskes, R.S. Thakur, P.K. Madhu, N.D. Kurur, S. Vega, Bimodal floquet description of heteronuclear dipolar decoupling in solid-state nuclear magnetic resonance, J. Chem. Phys. 127 (2007) 024501.
[12] R.S. Thakur, N.D. Kurur, P.K. Madhu, An analysis of phase-modulated heteronuclear dipolar decoupling sequences in solid-state nuclear magnetic resonance, J. Magn. Reson. 193 (2008) 77.
[13] R.S. Thakur, N.D. Kurur, P.K. Madhu, Pulse duration and phase modulated heteronuclear dipolar decoupling schemes in solid-state NMR, Proc. Ind. Nat. Sci. Acad. Springer Verlag (2009).
[14] R.S. Thakur, N.D. Kurur, P.K. Madhu, An experimental study of decoupling sequences for multiple-quantum and high-resolution MAS experiments in solid-state NMR, Magn. Reson. Chem. 46 (2008) 166.
[15] S. Vega, Floquet Theory, The Encyclopedia of Nuclear Magnetic Resonance, Wiley, London, 1995. p. 2011.
[16] M. Leskes, P.K. Madhu, S. Vega, Floquet theory in solid-state nuclear magnetic resonance, Prog. Nucl. Magn. Reson. Spectrosc. 57 (2010) 345.
[17] J.S. Waugh, Theory of broadband spin decoupling, J. Magn. Reson. 50 (1982) 30.
[18] U. Haeberlen, High resolution NMR in solids – selective averaging, Supplement – 1, Adv. Magn. Reson., Academic Press, New York, 1976.
[19] I. Scholz, P. Hodgkinson, B.H. Meier, M. Ernst, Understanding two-pulse phase-modulated decoupling in solid-state NMR, J. Chem. Phys. 130 (2009) 114510.
[20] G.J. Boender, S. Vega, H.J.M. De Groot, A physical interpretation of the Floquet description of magic angle spinning nuclear magnetic resonance spectroscopy, Mol. Phys. 95 (1998) 921.
[21] J.H. Van Vleck, On σ-type doubling and electron spin in the spectra of diatomic molecules, Phys. Rev. 33 (1929) 467.
[22] M. Veshtort, R.G. Griffin, SPINEVOLUTION: a powerful tool for the simulation of solid and liquid state NMR experiments, J. Magn. Reson. 178 (2006) 248.
[23] C. Augustine, N.D. Kurur, Heteronuclear dipolar decoupling in liquid-crystal NMR using supercycled SW$_f$-TPPM sequences, Magn. Reson. Chem. 48 (2010) 798.
[24] C.V. Chandran, P.K. Madhu, P. Wormald, T. Bräuniger, Frequency-swept pulse sequences for ^{19}F heteronuclear spin decoupling in solid-state NMR, J. Magn. Reson. 206 (2010) 255.
[25] S.K. Zaremba, Good lattice points, discrepancy, and numerical integration, Ann. Mat. Pura. Appl. 293 (1966) 4.
[26] H. Conroy, Molecular Schrödinger equation. VIII. A new method for the evaluation of multidimensional integrals, J. Chem. Phys. 47 (1967) 5307.
[27] V.B. Cheng, H.H. Suzukawa Jr., M. Wolfsberg, Investigations of a nonrandom numerical method for multidimensional integration, J. Chem. Phys. 59 (1973) 3992.